Extracting CFT data from Fixed Points of Higher Order Tensor Renormalization Group

Wenhan Guo[1] and Tzu-Chieh Wei[1]

[1] *C. N. Yang Institute for Theoretical Physics and Department of Physics and Astronomy, State University of New York at Stony Brook, Stony Brook, NY 11794-3840, USA*

(Dated: January 10, 2023)

In this paper we showed that the coarse-graining process in Higher Order Tensor Renormalization Group method preserves the information of operator insertion in UV. So the coarse-grained tensor not only describes the vacuum partition function of the corresponding IR theory, but also informations about low-energy excitations.

In particular, we shows that states corresponding to primary and descendent operators are the eigenvectors of linearized Tensor Renormalization Group. We also shows the position of operator-insertion in coarse-grained tensors can be reconstructed as a Taylor expansion in terms of descendant operators.

I. INTRODUCTION

A. Tensor Renormalization Group

Translation invariant tensor network is a natural way to describe the partition function of many statistical models and wave functions of quantum systems, such as the Ising model on a square lattice, and the ground-state wave function of the AKLT model. By replacing certain tensors by a "defect tensor", one can further compute the n-point expectation value or correlation function:

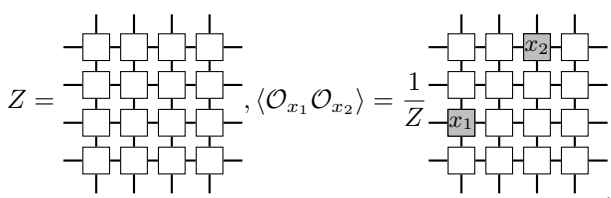

(1)

To evaluate the contraction of the tensor network eq1 on a large-scale lattice, which yields the vacuum partition function of the system at the continuum limit, one iteratively transforms the tensor network into a new tensor network on a coarse-grained lattice. It is called real-space Tensor Renormalization Group(TRG):

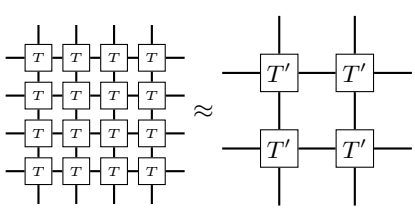

(2)

The bond dimension of the coarse-grained tensor will grow exponentially. To make it feasible for numerical computation, one needs to truncate the Hilbert space of the virtual degrees of freedom (i.e. bond dimensions) in each leg. Various numerical methods such as TRG [cite Levin and Nave], HOTRG [9], TNR [3, 4], SRG [10], GILT [6] are proposed.

B. Renormalization Group in CFT

On the other hand, the behavior of statistical and quantum systems at difference length scales can be described using the Renormalization Group (RG) Flow, as illustrated in Fig. 1.

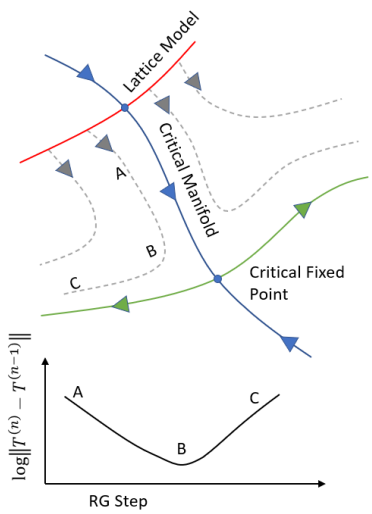

FIG. 1: Concept of Renormalization Group Flow.

At criticality the system flows into a certain type of fixed point which often can be described by a Conformal Field Theory (CFT), where there is an emergence of scale invariance at long distances, and the two-point functions follows the power law:

$$\langle \mathcal{O}_{x_1} \mathcal{O}_{x_2} \rangle \propto \frac{1}{(x_1 - x_2)^{2\Delta_{\mathcal{O}}}}, \tag{3}$$

where $\Delta_{\mathcal{O}}$ is the scaling dimension of the operator $\mathcal{O}$.

When the system is near the critical manifold, it will firstly converges to some place near the critical manifold, and then deviates from it exponentially, travelling to perhaps another fixed point, ss illustrated in Fig. 1. In Tensor Renormalization Group, the difference between

coarse-grained tensors from successive RG steps also follows a curve as illustrated in Fig. 1, which was reported in Refs. [4, 7]. That is we expect the change of the system after each RG transformation to behave as a V-shaped curve at the logarithm scale and, for example, the location B is the closest to a nearby critical manifold. As a result, the system can behave like different CFTs at corresponding length scales, dependent the detailed RG flow.

Note that $\mathcal{H}_v \otimes \mathcal{H}_v \cong \mathcal{H}_v$ implies $\dim\mathcal{H}_v = 1$ or ∞. So one have to bear in mind the truncation error from finite bond dimension when comparing tensors from different coarse-grained scales. Also note that the "virtual" Hillbert space $\mathcal{H}_v$ on the legs are unphysical, suffer from a $GL(D)^{\otimes m}$ gauge-redundancy, where D is the bond dimension and m is the spacetime dimension of the lattice. One have to adopt a proper gauge-fixing procedure in order to compare different tensors from different RG steps.

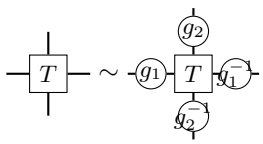

(4)

Very recently, it has been shown that one can iteratively transform the tensor into its Minimal Canonical Form (MCF) [1], which is unique up to a residue $U(D)^{\otimes m}$ gauge transformation.

C. Linearized Tensor Renormalization Group

If the truncation error is negligible, and gauge redundancy is properly fixed, T^l and T^{l+2} are similiar component-wise when the system is near the conformal fixed point. Then one can try to identify the Hillbert space of the unphysical, "virtual" bonds of T^l and T^{l+2}.

The linearized Tensor Renormalization Group[7] is defined as:

$$M^{i'j'k'l'}_{ijkl} = \frac{\partial T'^{i'j'k'l'}}{\partial T^{ijkl}} \tag{5}$$

At criticality, the eigenvalues λ_α of M gives the conformal dimension $\Delta_{\mathcal{O}_\alpha}$ of the CFT operators:

$$M\,|\mathcal{O}_\alpha\rangle = \lambda_\alpha\,|\mathcal{O}_\alpha\rangle \tag{6}$$

$$\frac{\lambda_\alpha}{\lambda_0} = s^{-\Delta_{\mathcal{O}_\alpha}}, \tag{7}$$

where $s = 2$ is the linear scaling of the system after one RG step.

Ref. [7] shows that one can obtain the scaling dimensions of the first few operators in the Ising CFT from the linearized HOTRG scheme with GILT and a partially gauge-fixing procedure. Morever, Ref. [3] also gives an amainzing result of the first 101 scaling dimensions of local and non-local operators in Ising CFT, using a much evolved TNR method.

In this paper, we will demonstrate that the corresponding eigenvectors $|\mathcal{O}_\alpha\rangle$ has a clear physical meaning. They are the conformal states, which is obtained by inserting conformal primaries and descendants into the vacuum state at origin. On the lattice level, the latter can be achieved by coarse graining the tensor network eq.1 with the operator insertion as defect tensors:

$$|\mathcal{O}_\alpha\rangle = \lim_{r\to 0} \mathcal{O}_\alpha(r)\,|0\rangle \approx \sigma_{x_1}\sigma_{x_2}\ldots\,|0\rangle_{\text{lattice}} \tag{8}$$

In this paper, we also show the two-point correlation function of the Ising model on the square lattice obtained by the TRG method. We argue that the position of operator in the coarse-grained defect tensor $T_{\sigma_{x_1}}$ is encoded by its projections on the primaries and descendants tensors.

II. MAIN RESULTS

A. Convergence onto the conformal fixed point in higher order tensor renormalization group

We observe that, with the removal of local entanglement using GILT[6] and gauge-fixing using MCF[1], there is a nontrivial fixed point of HOTRG[9], which corresponds to the Ising Conformal Field Theory $\mathcal{M}(3,4)$[2].

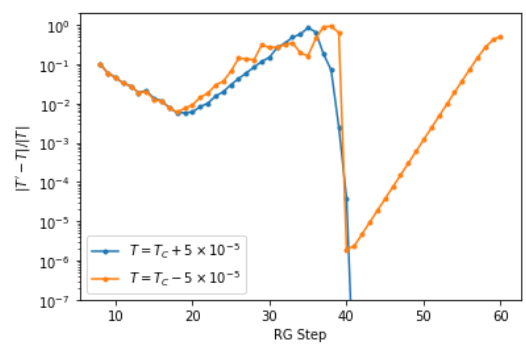

FIG. 2: The per-component difference of the coarse-grained tensor $||T^{(l)} - T^{(l-2)}||$ before and after every two layers of HOTRG coarse-graining for Ising model at $T = T_c + 5\times10^{-5}$ and $T = T_c - 5\times10^{-5}$. Both systems approaches the conformal fix point around layer 20. The low-temperature system then flows to the degenerated low-temperature fixed point around layer 46, then finally converges at the trivial fixed point. The high-temperature system directly converges at the trivial fixed point. Bond dimension $D = 32$, GILT is applied with $\epsilon_{\text{GILT}} = 8\times10^{-7}$, $\text{nIter}_{\text{GILT}} = 1$.

Figure 2 show the variation of the coarse-grained tensor $||T^{(l)} - T^{(l-2)}||$ of the 2D square lattice Ising model

near the critical temperature along HOTRG iterations. There is a fixed point around step 20. The system converges to the fixed point exponentially in steps 10-20, and then due to numerical error, deviates away from the fixed point exponentially in steps 20-40, featuring a V-shape curve in the logarithm plot.

B. Scaling Dimension from linearized tensor renormalization group

Table. I shows the scaling dimensions obtained by diagonalizing the transfer matrix on a cylinder and linearized Tensor Renormalization Group 5.

		with GILT		without GILT		Ref.[7]	
exact	Δ	Δ_{cyl}	Δ_{RG}	Δ_{cyl}	Δ_{RG}	Δ_{cyl}	Δ_{RG}
$\mathbb{1}$	0						
σ	$\frac{1}{8}$	0.1218	0.1350	0.1343	0.1518	0.125	0.127
ϵ	1	1.0061	0.9014	1.0094	1.0324	1.002	1.009
$\partial_x\sigma$,	$1+\frac{1}{8}$	1.1360	1.0713	1.1305	1.1392	1.128	1.125
$\partial_y\sigma$		1.1360	1.0639	1.1305	1.1376	1.128	1.128
$\partial_x\epsilon$,	2	2.0150	1.6623	2.0506	1.8903	2.014	2.002
$\partial_y\epsilon$,		2.0157	1.6671	2.0535	1.9032	2.014	2.004
T,		2.0157	1.7183	2.0711	1.9263	2.016	2.068
$\bar{T}$,		2.0166	1.7978	2.0711	1.9252	2.016	2.073
$\partial_{xx}\sigma$,	$2+\frac{1}{8}$	2.1373	1.7923	2.1933	1.9458		
$\partial_{xy}\sigma$,		2.1503	1.8074	2.2077	1.9413		
$\partial_{yy}\sigma$,		2.1510	1.9416	2.2639	2.0052		
		3.0294	2.0090	2.9642	2.0092		

TABLE I: The central charge and the first 10 scaling dimensions at RG Step 20 obtained from: 1. transfer matrix on a cylinder[5] Δ_{cyl}, 2. linearized tensor renormalization groupΔ_{RG}. Bond dimension $D = 24$, GILT is applied with $\epsilon_{\text{GILT}} = 8 \times 10^{-7}$, $\text{nIter}_{\text{GILT}} = 1$. In Ref.[7], Step=22, $D = 30$

C. Scaling Dimension from two-point correlators

Figures 3 and 4 show the two-point correlation function $\langle\sigma(0)\sigma(x,y)\rangle$ of the Ising model on a square lattice slightly above and below the critical temperature.

The points (x, y) are randomly sampled at the xy-plane. In fig. 34 correlation functions at different direction, which is indicated by the color of the data points, have the same distance dependency. It indicates that the $SO(2)$ rotational symmetry is restored at large distance.

We fit the scaling dimension from the low-temperature and high-temperature correlations function using the following ansatzes:

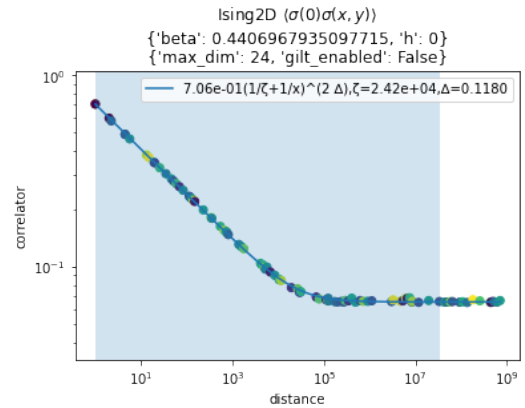

FIG. 3: The two-point correlator $\langle\sigma(0)\sigma(x,y)\rangle$ of the Ising model at $T \lesssim T_c$ on a square lattice obtained from coarse-graining defect tensors using HOTRG. Color denotes different angles $\arctan y/x$. The shaded region is used to fit the curve. Bond dimension $D = 24$, GILT is not adopted.

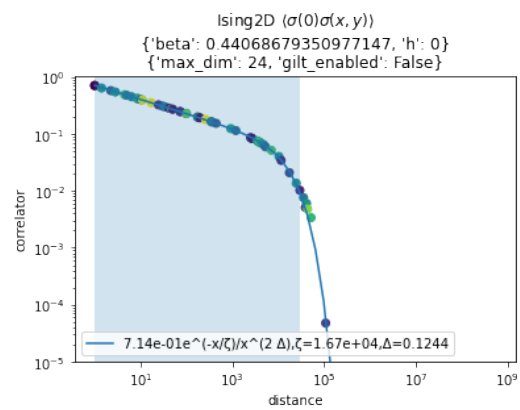

FIG. 4: The two-point correlator $\langle\sigma(0)\sigma(x,y)\rangle$ of the Ising model at $T \gtrsim T_c$ on a square lattice. Same parameters as Fig. 3

$$\langle\sigma(0)\sigma(x)\rangle = A\left(\frac{1}{\zeta}+\frac{1}{x}\right)^{2\Delta}, \tag{9}$$

$$\langle\sigma(0)\sigma(x)\rangle = A\frac{e^{-x/\zeta}}{x^{2\Delta}} + m_0^2, \tag{10}$$

$$\langle\sigma(0)\sigma(x)\rangle = A\frac{e^{-x/\zeta}}{x^{2\Delta}}, \tag{11}$$

where Δ is the scaling dimension of the magnetization operator σ, ζ is the correlation length, m_0 is the contribution of 1-point function.

The fitted scaling dimension is 0.1180 at low temperature limit with Ansatz 9 and 0.1224 at high temperature limit with Ansatz 11. The results confirm well with expected 1/8.

We also found that Ansatz 9 gives a slightly better

fit than Ansatz 10 for the low temperature correlation function. The physical meaning of 9 is to be understood.

D. Periodicity of two-point correlator on a torus

We claim that the information of the position of inserted operators are conserved during RG coarse graining steps. To demonstrate this, we calculate the two-point correlation function $\langle\sigma(0,0)\sigma(x,0)\rangle$ on a 1024×1024 torus using the HOTRG method, and results area shown in Fig. 5.

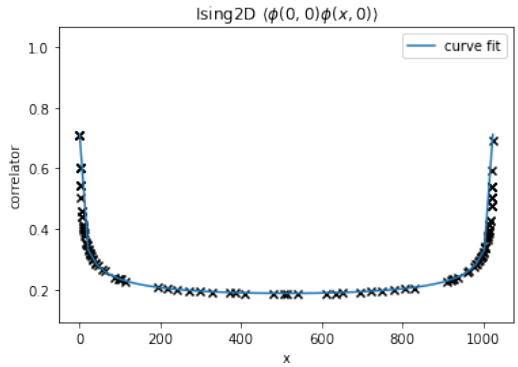

FIG. 5: The two-point correlator $\langle\sigma(0,0)\sigma(0,y)\rangle$ of the Ising model at $T \lesssim T_c$ on a 1024×1024 torus. Bond dimension $D = 24$, GILT is not adopted.

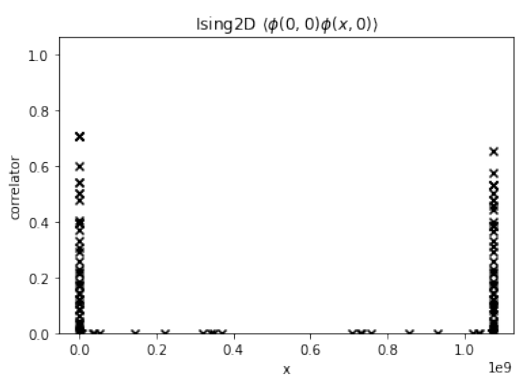

FIG. 6: The two-point correlator $\langle\sigma(0,0)\sigma(0,y)\rangle$ of the Ising model at $T \lesssim T_c$ on a $2^{30} \times 2^{30}$ torus. Same parameter as fig.5

It confirms well with the spin-spin correlation of the Ising CFT on a torus [2] (12.108):

$$\langle\sigma(0,0)\sigma(x,y)\rangle \propto \left|\frac{\partial_z\theta_1(0|\tau)}{\theta_1(z|\tau)}\right|^{\frac{1}{4}} \frac{\sum_{\nu=1}^{4}|\theta_\nu(z/2|\tau)|}{\sum_{\nu=2}^{4}|\theta_\nu(0|\tau)|}, \quad (12)$$

where $z = \frac{1}{L_x}(x+iy)$ is the complex coordinate, L_x, L_y are the size of the lattice, $\tau = iL_y/L_x$, and θ_ν's are the elliptic theta functions. We follow the convention that θ_ν are (anti)periodic in $z \to z+1$ and quasiperiodic in $z \to z+\tau$.

As expected, there is a periodic behavior of the two-point function $\langle\sigma(0,0)\sigma(x,0)\rangle$ as x goes through the entire torus. Numerically, it is a nontrivial result, because the correlation function is very sensitive to the change of x when $x \to L \gg 1$.

However, the two 1-pt coarse-grained tensors T_{σ_0} and T_{σ_x} do not meet until the very late step of RG coarse graining. Since in most TRG scheme, coarse-grained tensor $T_{\sigma_0\sigma_x}$ has no prior knowledge of global topology, they have to record x to a precision $\mathcal{O}(1/L)$ in order to represent the sharp response at $x \to L$. It suggests that the information about the position x of operator insertion is not lost or smeared during all the coarse-grain steps.

Fig.6 shows the two-point function on a much larger torus, corresponding to 60 layers. since the system had already flow away from conformal fixed point around layer 20, as shown in Fig.2,44, one would not expect the correlation function satisfies eq.12. However, Fig.6 shows an astonishing result that after nearly 1073741824 lattice sites, the two-point function goes up again within just a few lattice sites. Which means the position of operator insertion is preserved in the coarse-grained tensor up to an precision of 10^{-9}, at least when near the boundary. In secII F we will shown that the position information, defined on a discrete lattice, is stored as a continuous-valued component of the coarse-grained tensor.

E. Comparision of eigenvectors of linearized TRG and coarse-grained tensors with operator insertion

We claim that the eigenvectors of linearized TRG matrix 5 has an explicit physical meaning: they are states of conformal primaries and descendants. To show this, we compare the coarse-grained tensors with operator insertion $T_{\sigma_{x_1}\sigma_{x_2}\ldots}$ with the first few eigenvectors v_i of linearized TRG eq.5 near the conformal point as shown in Fig.7.

The coarse-grained vacuum tensor T lies on the eigenspace with conformal dimension 0, which corresponds to the identity operator $\mathbb{1}$.

The coarse-grained tensor with 1 operator insertion T_{σ_x} lies on the eigenspace of conformal dimension 0.125, which corresponds to the spin operator σ. As shown in the figure. Note that there are leff significant projection on higher eigenvectors. They are either the numerical error, or an result that the operator insertion position is not exactly in the middle.

The coarse-grained tensor with 2 operator insertion $T_{\sigma_{x_1}\sigma_{x_2}}$ lies both on $\Delta = 0$ and $\Delta = 1$. it confirms with the fusion rule of ising CFT: $\sigma \times \sigma = \mathbb{1} + \epsilon$. ϵ is the energy density operator with $\Delta = 1$.

The coarse-grained tensor with 3 operator insertion $T_{\sigma_{x_1}\sigma_{x_2}\sigma_{x_3}}$ further confirms with the fusion rule $\epsilon \times \sigma = \sigma$ and $\mathbb{1} \times \sigma = \sigma$.

Note that there are undesired projection on $\Delta \gtrsim 2$.

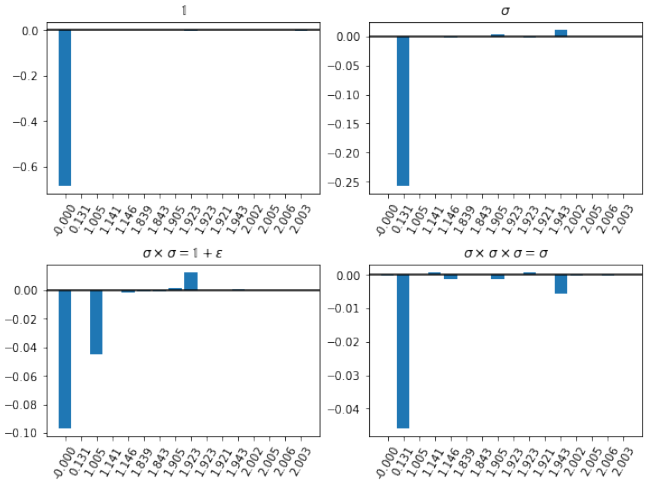

FIG. 7: Projection of coarse-grained tensors with operator insertion onto eigenvectors of linearized TRG at RG Step 20. Bond dimension $D = 30$, GILT is not adopted.

We further compare the other eigenvectors with the conformal descendants obtained by finite-differencing coarse-grained tensors with different operator insertion positions. The scheme is elaborated in tableII, and the results are shown in fig. 8.

coarse-grained tensor	Δ	inserted operator at lattice level
$\mathbb{1}$	0	$\mathbb{1}$
σ	1/8	$\sigma_{0,0}$
$\sigma\times\sigma=\mathbb{1}+\epsilon$	0,1	$\sigma_{l,0}\sigma_{-l,0}$
$\sigma\times\sigma\times\sigma=\sigma$	1/8	$\sigma_{l,0}\sigma_{-\frac{1}{2}l,\frac{\sqrt{3}}{2}l}\sigma_{-\frac{1}{2}l,-\frac{\sqrt{3}}{2}l}$
$\partial_x\sigma$	1+1/8	$(\sigma_{d,0}-\sigma_{-d,0})$
$\partial_y\sigma$	1+1/8	$(\sigma_{0,d}-\sigma_{0,-d})$
$\partial_x\epsilon$	2	$(\sigma_{d,l}\sigma_{d,-l}-\sigma_{-d,l}\sigma_{-d,-l})$
$\partial_y\epsilon$	2	$(\sigma_{l,d}\sigma_{-l,d}-\sigma_{l,-d}\sigma_{-l,-d})$
$T_\times$	2	$(\sigma_{l,l}\sigma_{-l,-l}-\sigma_{l,-l}\sigma_{-l,l})$
T_+	2	$(\sigma_{l,0}\sigma_{-l,0}-\sigma_{0,l}\sigma_{0,-l})$
$\partial_x^2\sigma$	2+1/8	$(\sigma_{d,0}-\sigma_{d',0}-\sigma_{-d',0}+\sigma_{-d,0})$
$\partial_y^2\sigma$	2+1/8	$(\sigma_{0,d}-\sigma_{0,d'}-\sigma_{0,-d'}+\sigma_{0,-d})$
$\partial_x\partial_y\sigma$	2+1/8	$(\sigma_{d,d}-\sigma_{-d,d}-\sigma_{d,-d}+\sigma_{-d,-d})s$

TABLE II: Coordinates and patterns of operator insertion for fig.78

From fig. 8 we found that $\partial_x\sigma$ and $\partial_y\sigma$ forms a nearly degenerate 2-dimensional subspace of $\Delta \approx 1$. The other descendants such as ($T_\times$, T_+) and ($\partial_x\epsilon$, $\partial_y\epsilon$, $\partial_x\partial_y\sigma$) are also grouped together in each subspaces with dimension 2 and 3. Unfortunately, due to numerical error, the order of eigenvalues are wrong. Note that ideally $\Delta_T = 2$ and $\Delta_{\partial^2\sigma} = 2.125$.

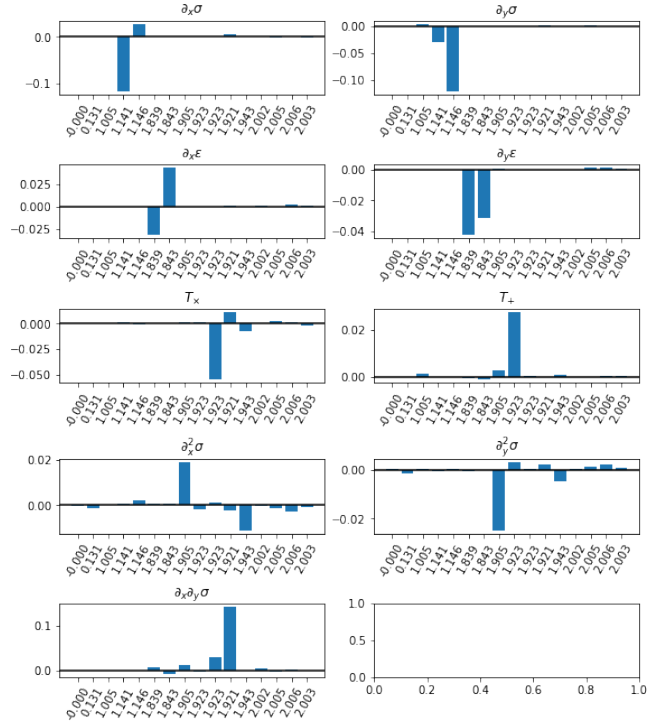

FIG. 8: Finite Difference of coarse-grained tensors onto eigenvectors of linearized TRG. Same parameter as 7

F. Encoding of the position of operator insertion in coarse-grained tensors

We find that in 1-pt tensor $T_{\sigma_{x,0}}$, the position x of operator insertion is encoded in the subspace spanned by $\partial\sigma$, $\partial^2\sigma$, ..., as suggested by the Taylor Expansion:

$$\sigma(x,y) = \sigma(0,0) + x\partial_x\sigma(0,0) + y\partial_y\sigma(0,0) \tag{13}$$

$$+\frac{1}{2}(x^2\partial_x^2\sigma(0,0) + xy\partial_x\partial_y\sigma(0,0) + y^2\partial_y^2\sigma(0,0)) + ... \tag{14}$$

Fig.9 shows the decomposition of $T_{\sigma_{x,0}}$ onto the conformal tensors σ, $\partial\sigma$, $\partial^x\sigma$. The conformal tensors are obtained by fixing the rotation of eigenvectors $|u_a\rangle$ of lTRG M using method described in Appendix B.

We do not directly compare $T_{\sigma_{x,0}}$ with the coarse-grained tensors T_σ, $T_{\partial\sigma}$... It is because as suggested by [11], the higher-indice components of the coarse-grained tensor, or equivalently, the subspace spanned by less significant eigenvectors, are the unphysical 'noise' of bond-dimension truncation and numerical errors. So we only do the comparison in the subspace spanned by the most significant eigenvectors.

From fig.9 we see that, as the operator $\sigma(x)$ moves along the x-axis, its projection on $T_{\partial_x\sigma}$ changes linearly, and its projection on $T_{\partial_x^2\sigma}$ changes quadratically. Also its projection on T_σ remains almost constant. It confirms with the Taylor expansion 14.

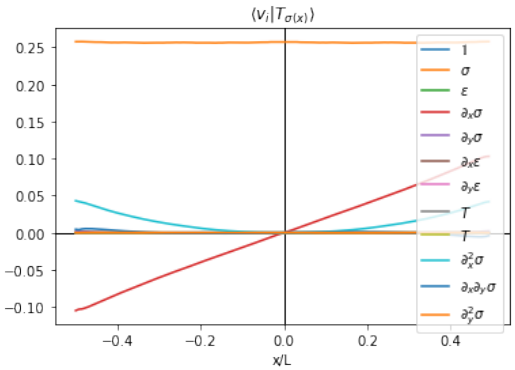

FIG. 9: Projection of coarse-grained tensor with different operator insertion positions onto the conformal state. $L = 1024$ the lattice size. Same parameter as 7

III. COMPARISON OF COARSE-GRAINING WITH AND WITHOUT GILT

Here we show that, although Graph Independent Local Truncation (GILT) gives better results in quantities which only dependents on the free energy Z, such as scaling dimensions Δ and central charge c, and makes it possible for the coarse-graining steps to keep stable in the critical regime, GILT should not be used in tasks involving coarse-graining defect tensors, such as the N-point correlation functions.

The truncation matrix R obtained from GILT only guarantees the local tensor is not changed if all the tensors on the local sites are vacuum tensors. What GILT truncates on the boundary Hillbert space is the subspace which corresponds to defect tensors. It can be argued by the fact that the local entanglement GILT truncates have contribution to n-point correlators for the sites near the boundary.

Fig.10 shows the per-component difference, scaling dimensions and central charge, obtained from successive coarse-grained tensors in RG procedure with and without GILT.

Fig.10a) shows TRG without GILT failed to converge to the fixed point at criticality.

In fig.10b,c), the central charge and scaling dimensions have an unstable oscillation starts from layer 10. The oscillation can be explained by that we are doing horizontally and vertically coarse-graining on the alternative RG steps. So the coarse-grained tensors with odd step number are corresponds to a rectangular region with aspect ratio $2:1$. We have to change TODO accordingly when calculating c and Δ from diagonalizing the transfer matrix. In HOTRG without GILT, the local entanglement, which can be parameterized by CDL tensors, will gradually take up the coarse grained tensor. The CDL tensor does not responds to change of aspect ratio, which results in a period-2 oscillation in Δ and c. We further conclude that the oscillation is a good benchmark to see when the coarse-graining method starts to lose its fidelity and

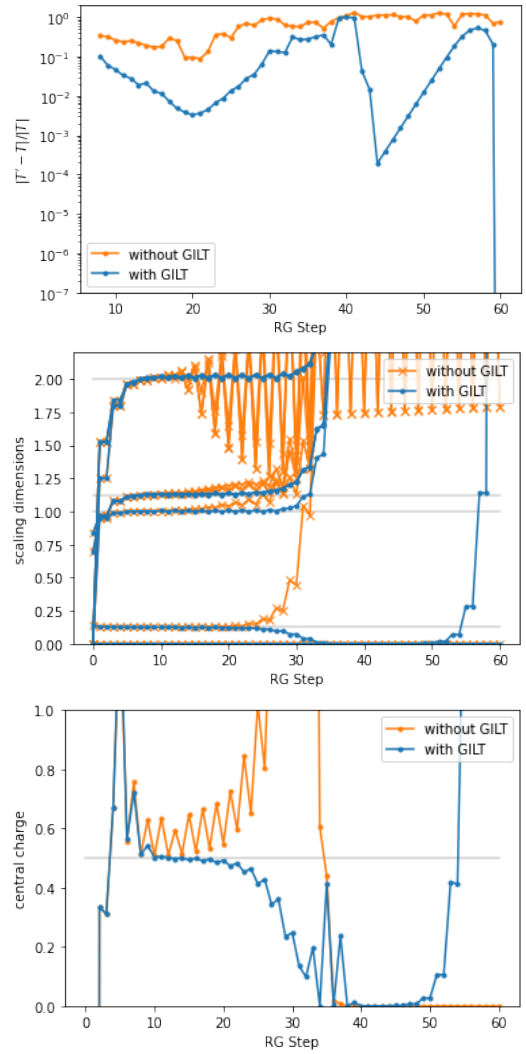

FIG. 10: Comparison of HOTRG with and without GILT. a) Per-component difference of coarse-grained tensors from successive RG steps. b,c) scaling dimensions and central charge obtained from diagonalizing transfer matrix. Bond dimension $D = 24$, $\epsilon_{\text{GILT}} = 8 \times 10^{-7}$, $\text{nIter}_{\text{GILT}} = 1$.

whether the entanglement filtering method has cleaned up the CDL tensors.

The two-point correlator $\langle \sigma(0)\sigma(x) \rangle$ obtained from HOTRG with GILT has a wrong scaling dimension, as shown in FIg.11. The correlation function of HOTRG+GILT decays faster than expected value. It might be explained by that the defect tensor are being partially truncated by GILT at each RG step. Note that the two schemes flows to different phases at critical temperature. One just compare the part before the system flows away from critical points.

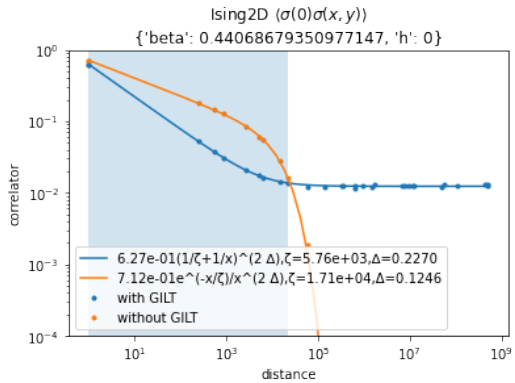

FIG. 11: Comparison of HOTRG with and without GILT in 2-point correlator. Same parameter as fig.10. Note that the two schemes flows to different phases.

IV. METHODS

A. Coarse-graining the Vacuum Tensor

Here is the coarse-graining steps we used in this paper:

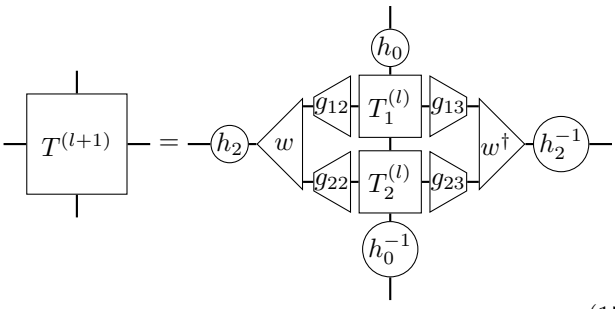

(15)

We do the vertical and horizontal coarse-graining steps alternatively. At each coarse-graining layer, w, $w^\dagger$ are the isometries obtained using HOTRG. g_{12}, g_{13}, g_{22}, g_{23} are the entanglement truncation matrix obtained using GILT. h_0, h_2 are the gauge-fixing matrix obtained using MCF and sign-fixing.

The idea of HOTRG is to find a coarse-grained tensor T' and isometries $w{:}\mathcal{H}_v \to \mathcal{H}_v \otimes \mathcal{H}_v$, which can mimic the original tensor subnetwork as much as possible:

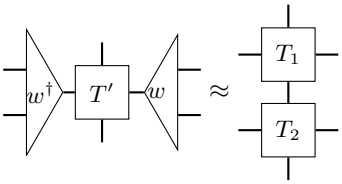

(16)

Vanilla HOTRG suffers from the microscopic entanglement between the pair of sites next to the boundary of coarse-grained regions. To capture the long-range behavior of the system using a tensor with finite bond dimension, local entanglement removal must be done. On a square lattice, local entanglement can be parametrized by corner-double-line (CDL) tensors. Which can be removed by Graph Independent Local Truncation (GILT).

The idea of GILT is to modify a subset of tensor network such as a plaquette, so as the modified subnetwork still looks the same from external legs, but the entanglement through a certain internal leg is reduced:

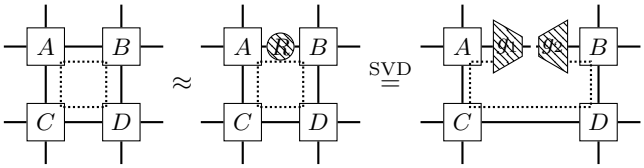

(17)

One have to enumerate all the possible plaquette-leg combinations in order to remove all the local entanglements. In practice, as suggested by [7], it is sufficient to only apply on the following plaquette-legs:

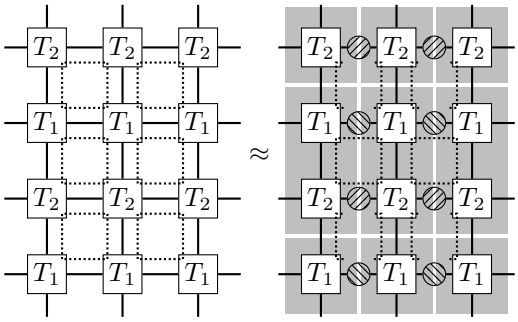

(18)

The tensor in the gray shade is to be coarse-grained, with circle-shaped GILT tensors being splitted using SVD. We only truncate half of the CDL loops across the legs to be coarse-grained.

The prescription of HOTRG (alg.1), GILT(alg.2), MCF(alg.3), sign-fixing(alg.4) are listed in the appendixA.

B. Coarse-graining the Defect Tensor

We use the same set of coarse-graining tensors w, g, h from coarse-graining vacuum tensors, to coarse-grain the network with insertion of defect tensors.

Similarly, when calculating linearized TRG eq.5, we keep the coarse-graining tensors w, g, h as constants, i.e. their variation with respect to change of the input tensor is discarded.

As a result, the coarse-grained tensor is quad-linear in the four input tensors (in the following equation, the isometries w and truncations g are omitted):

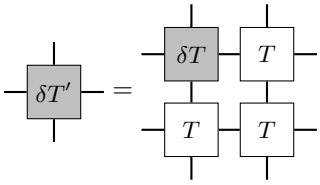

+ 3 other terms (19)

As shown in Sec.III, one can get faithful scaling dimensions from linearized TRG with fixed g and w. However, in terms of n-point correlation functions, one gets undesirable results if GILT is applied.

It is because GILT equation A5 holds only when the tensors $ABCD$ in the subnetwork eq. A5 are all vacuum tensors. Actually, one may question whether the Hillbert space GILT truncates is the subspace which corresponds to defect tensors.

HOTRG instead can guarantee the fidelity of 1-point correlation functions. Note that the HOTRG equation eq16 holds if both T_1 and T_2 are vacuum tensors. So, the environment E of a defect tensor $T_{\mathcal{O}}$, which is the contraction of the tensor network with $T_{\mathcal{O}}$ removed and only contains vacuum tensors, can be faithfully computed using HOTRG coarse-graining method.

For two-point functions and more. The environment can still be obtained from coarse-graining the remaining vacuum tensor. The source of error comes from the insertion of $w^\dagger w$ between two coarse-grained defect tensors. Note that $w^\dagger w \simeq \mathbb{1}$ holds only if either the left side or the right side are concatenated with only vacuum tensors.

One can see the coarse-graining tensor network with w, g, h insertion as a tree-like tensor network ansatz which tries to fit the ground state wavefunction. As suggested by MERA[8], disentanglers are required to faithfully represent the ground state wave function of a critical system. In our ansatz, we only have truncation instead of disentanglers.

So, one possible improvement is to use coarse-graining methods such as TNR[4] which introduces disentanglers into the coarse-graining network.

Another possible improvement is to use different g and w when coarse-graining defect tensors.

V. CONCLUSION

In this paper we shows one can get JKLDSAJKLDJFSKLJKFLDSJLKSDJFKL from

VI. ACKNOWLEDGEMENTS

TIKZ Manual TIKZ Ref GILT Paper MCF Paper
Nikko and our Funding

[1] A. Acuaviva, V. Makam, H. Nieuwboer, D. Pérez-García, F. Sittner, M. Walter, and F. Witteveen. The minimal canonical form of a tensor network. 9 2022.

[2] P. Di Francesco, P. Mathieu, and D. Senechal. *Conformal Field Theory*. Graduate Texts in Contemporary Physics. Springer-Verlag, New York, 1997.

[3] G. Evenbly. Algorithms for tensor network renormalization. *Physical Review B*, 95(4):045117, 2017.

[4] G. Evenbly and G. Vidal. Tensor network renormalization. *Physical review letters*, 115(18):180405, 2015.

[5] Z.-C. Gu and X.-G. Wen. Tensor-entanglement-filtering renormalization approach and symmetry-protected topological order. *Phys. Rev. B*, 80:155131, Oct 2009.

[6] M. Hauru, C. Delcamp, and S. Mizera. Renormalization of tensor networks using graph independent local truncations. *Phys. Rev. B*, 97(4):045111, 2018.

[7] X. Lyu, R. G. Xu, and N. Kawashima. Scaling dimensions from linearized tensor renormalization group transformations. *Phys. Rev. Res.*, 3(2):023048, 2021.

[8] G. Vidal. Class of quantum many-body states that can be efficiently simulated. *Phys. Rev. Lett.*, 101:110501, Sep 2008.

[9] Z. Y. Xie, J. Chen, M. P. Qin, J. W. Zhu, L. P. Yang, and T. Xiang. Coarse-graining renormalization by higher-order singular value decomposition. *Phys. Rev. B*, 86:045139, Jul 2012.

[10] Z. Y. Xie, H. C. Jiang, Q. N. Chen, Z. Y. Weng, and T. Xiang. Second renormalization of tensor-network states. *Physical Review Letters*, 103(16), Oct 2009.

[11] S. Yang, Z.-C. Gu, and X.-G. Wen. Loop optimization for tensor network renormalization. *Phys. Rev. Lett.*, 118:110504, Mar 2017.

Appendix A: List of Algorithms

Algorithm 1 Higher Order Tensor Renormalization Group[9]

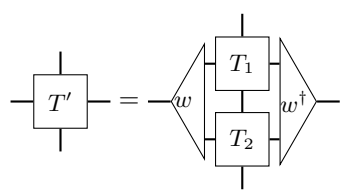

(A1)

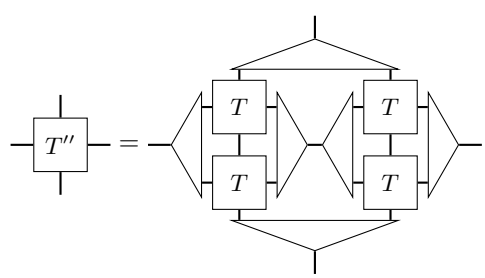

(A2)

Inputs: A translational invariant tensor network on a lattice. The tensor on each site is T.

Outputs: The coarse-grained tensor T' by grouping every two adjacent tensors in the chosen spacial dimension, and an isometry w which truncates the bond dimension of the coarse-grained tensor from $D \times D$ to D.

Steps:

To minimize the truncation error:

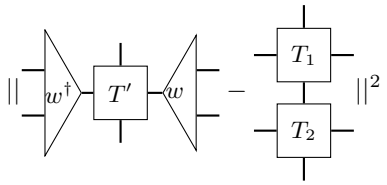

(A3)

The isometry w can be estimated from the singular value decomposition of the two-site reduced density matrix M:

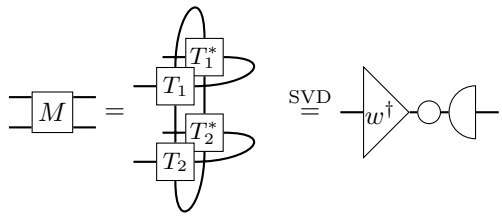

(A4)

On a 2D square lattice, one do the vertical and horizontal coarse-graining step alternatively, as shown in eq. A1.

Algorithm 2 Graph Independent Local Truncation[6]

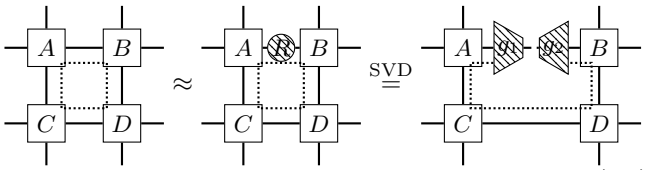

(A5)

Inputs: a subgraph of a tensor network, and an edge in the subgraph to truncate.

Outputs: a truncation matrix R to insert in the chosen edge, or equivalently, a pair of linear transformations g_1 and g_2, $R = g_1 g_2$ to apply to the legs of the adjacent tensors, that partially removes the local entanglements passing through the edge.

Steps:

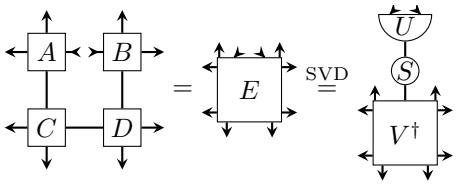

(A6)

The environment E of an edge is defined by removing that edge from the tensor network. E is interpreted as an isometry from the two ends of broken edges to the external edges.

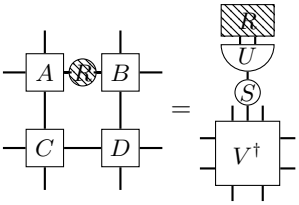

(A7)

By spectral decomposing E, one can see that the subspace of variations of $R \in \mathrm{Mat}_{D\times D}$ which does not significantly affect the tensor output, is spanned by the singular vectors corresponding to smaller singular values.

In particular, we choose R in the following way:

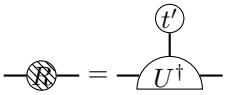

(A8)

$$t'_i = t_i \frac{\hat{S}_i^2}{\hat{S}_i^2 + \epsilon^2}, \hat{S}_i = \frac{S_i}{\max(S)},$$

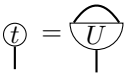

(A9)

Split R into g_1 and g_2 by SVD, and absorb them into the adjacent tensors, as in eq.A5.

One can further truncate the local entanglement by repeating the process on edge between g_1 and g_2.

Algorithm 3 Minimal Canonical Form[1]

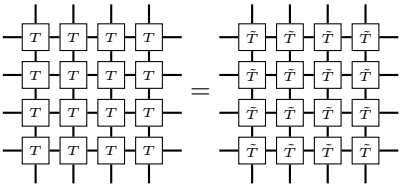

(A10)

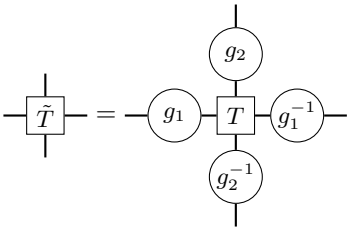

(A11)

Inputs: A translational invariant tensor network on a lattice. The tensor on each site is T.

Outputs: A linear transformation $(g_1, g_2) \in GL(D)^{\otimes m}$, which gauge transforms the tensor into its minimal canonical form:

$$T_{min} = \mathrm{argmin}\{||\tilde{T}||_2 : \tilde{T} \in \overline{G \cdot T}\} \tag{A12}$$

where m is the spacial dimension of the lattice, D is the bond dimension, $\overline{G \cdot T}$ is the closure of the gauge orbit generated by the gauge transform A11.

Steps:

The object to minimize is:

$$||T||_2 = \operatorname{tr} \rho = \operatorname{tr} |T\rangle \langle T| = \tag{A13}$$

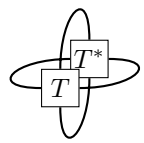

Its first-order variation with respect to gauge transformation is:

$$\partial_{t=0} ||(e^{tX_1}, e^{tX_2}) \cdot T||_2^2 = 2 \sum_{k=1}^{m} \operatorname{tr} X_k (\rho_{k,1} - \rho_{k,2}^T) \tag{A14}$$

where the reduced density matrices $\rho_{k,1}$,$\rho_{k,2}$ are:

$\rho_{1,1} =$ 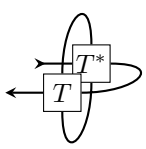

$, \rho_{1,2}^T =$ 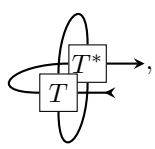

$,$

$\rho_{2,1} =$ 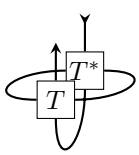

$, \rho_{2,2}^T =$ 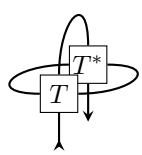

$,$ (A15)

According to [1], the global minimum can be reached by gradient descent. We apply the following gauge transform by the gradient in eq.A14 and the step length suggested in [1].

$= e^{-\frac{1}{4m}\frac{1}{tr\rho}(\rho_{k,1} - \rho_{k,2}^T)}$ (A16)

and repeat the whole process until converges.

Algorithm 4 Preliminary procedure of fixing the $U(1)$ gauge

After fixing the $GL(D)^{\otimes m}$ gauge using MCF, there's a remaining $U(D)^{\otimes m}$ gauge. In practice, it[7] shows that one only need to fix its $U(1)^{\otimes Dm}$ subgroup. For real tensors, which is just the sign-flipping on each indices of every legs.

Here shows our preliminary procedure to partially fix the $U(1)$ gauge

Input: T_{ijkl}, the tensor to be gauge-fixed. $\tilde{T}_{ijkl}$, the reference tensor for the gauge choice

Output: T_{ijkl}, the gauge fixed tensor

Steps:

for $d \leftarrow 1$ to $2D$ **do**

  $\rho_{1,i} \leftarrow \sum_{j,k,l \leq \min d,D} T_{ijkl} \tilde{T}_{ijkl}$

  $d_{1,i} \leftarrow \operatorname{sgn} \rho_{1,i}$

  $T_{ijkl} \leftarrow T_{ijkl} d_{1,i} d_{1,j}$

  do the same thing for other pairs of legs

end for

Appendix B: Fixing the rotation of conformal states

From linearized TRG M we obtain its 'raw' eigenvectors and eigenvalues:

$$M |u_a\rangle = \lambda_a |u_a\rangle \tag{B1}$$

Ideally they should correspond to the conformal states:

$$|\mathcal{O}_\alpha\rangle \in \{|\mathbb{1}\rangle, |\sigma\rangle, |\epsilon\rangle, |\partial\sigma\rangle, ...\} \tag{B2}$$

However, states share the same conformal dimension will mixed into each other. Also, due to numerical errors, states with different conformal dimensions might also mixed into each other in worse cases. So one have to rotate the basis $|u_a\rangle$ to build the conformal states $|\mathcal{O}_\alpha\rangle$:

$$|\mathcal{O}_\alpha\rangle = \sum_{\lambda_a = \Delta} S_{\alpha a} |u_a\rangle \tag{B3}$$

We use the scheme described in Table II to build the lattice implementation of conformal operators using finite-difference method and operator fusion. $|T_\alpha\rangle$ are the corresponding coarse-grained tensors. Notice that $|T_\alpha\rangle$ contains higher states in the conformal tower of $\mathcal{O}_\alpha$. For example:

$$\left|T_{\partial_x \sigma(x_0)}\right\rangle \sim \frac{1}{2\delta}(\sigma(x_0 + \delta) - \sigma(x_0 - \delta)) |0\rangle \tag{B4}$$

$$\sim |\partial_x \sigma(x_0)\rangle + \frac{1}{6} \left|\partial_x^3 \sigma(x_0)\right\rangle + ... \tag{B5}$$

The matrix S' consists the dot product between $|u_a\rangle$ and $|T_\alpha\rangle$:

$$S'_{a\alpha} = \langle u_a | T_\alpha \rangle \tag{B6}$$

We expect the block-diagonal part of S' corresponds to the inverse of rotation matrix, and the off-block-diagonal part are the higher terms correspond to finite-difference error. Then we can obtain the rotation matrix.

$$S^{(\Delta)} = S'^{(\Delta),-1} \tag{B7}$$

Where (Δ) means restricted on eigenspace $\lambda_\alpha, \lambda_a \approx \Delta$.

Note that in worst case when states with different scaling dimensions, such as $\Delta = 2$ and $\Delta = 2.125$ mixed into each other, due to poor numerical resolution, on have to rotate the two subspaces together.

Also, in worst case that the expected eigenvectors spreads into multiple eigenspaces, as shown in Fig.8, we use the pseudo-inverse on the rectangular sub-matrix.

In practice we found assuming all the eigenvectors are somehow mixed, i.e. do the pseudo-inverse for the whole matrix, gives best result.